Stability of squares and rolls in Rayleigh–Bénard convection in an infinite-Prandtl-number fluid between slabs

By B. HOLMEDAL

Department of Materials Technology, Norwegian University of Science and Technology,
N-7491 Trondheim, Norway

Nonlinear solutions in the form of squares and rolls are investigated for Rayleigh–Bénard convection in an infinite-Prandtl-number fluid enclosed between two symmetric slabs. It is found that the heat transfer depends strongly on the thickness and thermal conductivity of the slabs, but hardly on the planform of convection. Examples of stability regions of rolls are calculated, showing that for certain slab selections, rolls remain stable at even larger Rayleigh numbers than with fixed temperatures at the boundaries. The region of stable squares is restricted by a zigzag and a long-wavelength cross-roll instability in addition to a new three-dimensional instability. As the slab conductivity is increased, the stability region of the squares shrinks onto a point located well above the critical point for the onset of convection. For a small range of slab conductivities, stability regions for squares and rolls both exist for the same set-up. In the present calculations, the regions never overlap. An example, where both patterns are stable at the same Rayleigh number, provides an explanation for the co-existence of rolls and squares where transparent slabs with a low thermal conductivity were applied.

1. Introduction

Rayleigh–Bénard convection in a thin horizontal fluid layer enclosed between heat-conducting slabs is an ideal and simple pattern-generating configuration. A large amount of work has been devoted to the special case where the temperature is kept constant at the fluid boundaries, which can be experimentally achieved by applying well-conducting slabs. At the onset of convection, the stable pattern is then two-dimensional rolls, their fully nonlinear stability regions were first calculated by Busse (1967). Finite-Prandtl-number fluids yield more complex regions owing to the viscous instabilities (references may be found in Getling 1998). Frick, Busse & Clever (1983) showed that squares are unstable, and Clever & Busse (1996) found that hexagons are stable for supercritical Rayleigh numbers as low as 3000.

When taking into account slabs of finite heat conductivity, squares may be a stable pattern as well. This was first predicted for weakly supercritical Rayleigh–Bénard convection by Busse & Riahi (1980) and Proctor (1981), and the corresponding wavenumber restrictions by Hoyle (1993) for the asymptotic case of poorly conducting slabs, where the wavenumber becomes a small parameter. Correspondingly, various combinations of slab thicknesses and conductivities have been reported, references may be found in Holmedal, Tveitereid & Palm (2005), who concluded that the instability mechanisms are always similar to those reported by Hoyle (1993), and

that hexagons and all other patterns involving more than two modes are always unstable. Experimentally, evidence of the squares was reported by Le Gal, Pocheau & Croquette (1988).

The weakly nonlinear perturbation techniques are restricted to small Rayleigh numbers and degenerates for slab conductivities corresponding to the border between stable rolls and squares. For cases of infinitely thick heat-conducting slabs, fully nonlinear solutions and their heat transfer and stability regions were reported by Westerburg & Busse (2001). They found that the stability region shrinks onto the critical point for onset of convection as the slab the conductivity decreases. In an experiment they observed the coexistence of squares and rolls.

Realistic set-ups involving symmetric slabs of finite thickness and thermal conductivity are considered in the current investigation. Stability regions and heat transfer are calculated for both rolls and three-dimensional squares. Of special interest are cases with slab properties close to the transition between stable rolls and stable squares, where the weakly nonlinear theory does not apply. Beyond the weakly nonlinear range, hexagons are likely to be another stable solution not included here. Furthermore, infinitely large Prandtl numbers are assumed.

2. Mathematical formulation

A fluid layer of infinite horizontal extent and of constant depth h is considered. The thermal conductivity k and the thermal diffusivity κ are constant properties. The coefficient of thermal expansion β describes the linear density dependence on temperature. The fluid is bounded by two rigid heat-conducting slabs. The slabs have equal thickness denoted by $h^{(s)}$, thermal conductivity $k^{(s)}$ and thermal diffusivity $\kappa^{(s)}$.

The fluid is heated from below and cooled from above. The temperature is fixed at the outer boundaries of the slabs, and the temperature difference between these two boundaries is ΔT (positive).

To describe the geometry and the flow, Cartesian co-ordinates (x, y, z) are used. The z-axis is directed upwards, with the origin located at the centre of the fluid layer. In the governing equations, the density is regarded as constant except in the buoyancy term. A simple hydrostatic solution exists with a linear temperature variation in the vertical direction. The hydrostatic temperature difference between the top and the bottom of the fluid layer, $\Delta T^{(f)}$, then is:

$$\Delta T^{(f)} = \frac{K\,\Delta T}{2H + K},\tag{2.1}$$

where

$$H = h^{(s)}/h, \quad K = k^{(s)}/k.\tag{2.2}$$

A temperature perturbation θ, a pressure perturbation p and a fluid motion $\boldsymbol{v}$ of the hydrostatic solution is considered. The corresponding temperature perturbations in the slabs are denoted $\theta^{(l)}$ and $\theta^{(u)}$. The temperatures are made dimensionless by $\Delta T^{(f)}$. By using h, h^2/κ, κ/h and $\kappa\nu\rho_0/h^2$ as units of length, time, velocity and pressure, respectively, the equations are made non-dimensional. For cases of infinite Prandtl number, the horizontal components of the dimensionless velocity may be written as

$$(v_x, v_y, v_z) = \left(\frac{\partial^2 \psi}{\partial x \partial z}, \frac{\partial^2 \psi}{\partial y \partial z}, -\frac{\partial^2 \psi}{\partial x^2} - \frac{\partial^2 \psi}{\partial y^2} \right),\tag{2.3}$$

The governing dimensionless equations then take the form

$$\nabla^4 \psi - Ra\,\theta = 0, \tag{2.4}$$

$$\nabla^2 \theta - \frac{\partial^2 \psi}{\partial x^2} - \frac{\partial^2 \psi}{\partial y^2} = \frac{\partial \theta}{\partial t} + \frac{\partial^2 \psi}{\partial z \partial x}\frac{\partial \theta}{\partial x} + \frac{\partial^2 \psi}{\partial z \partial y}\frac{\partial \theta}{\partial y} - \left(\frac{\partial^2 \psi}{\partial x^2} + \frac{\partial^2 \psi}{\partial y^2}\right)\frac{\partial \theta}{\partial z}, \tag{2.5}$$

$$\nabla^2 \theta^{(l)} = \frac{\kappa}{\kappa^{(s)}}\frac{\partial \theta^{(l)}}{\partial t}, \tag{2.6}$$

$$\nabla^2 \theta^{(u)} = \frac{\kappa}{\kappa^{(s)}}\frac{\partial \theta^{(u)}}{\partial t}, \tag{2.7}$$

with boundary conditions

$$z = \pm\left(\tfrac{1}{2} + H\right): \quad \theta^{(l,u)} = 0, \tag{2.8}$$

$$z = \pm\tfrac{1}{2}: \quad \psi = \frac{\partial \psi}{\partial z} = 0, \quad \theta = \theta^{(l,u)}, \quad \frac{\partial \theta}{\partial z} = K\frac{\partial \theta^{(l,u)}}{\partial z}. \tag{2.9}$$

Here Pr and Ra are the Prandtl number and the Rayleigh number, respectively, defined by

$$Pr = \frac{\nu}{\kappa}, \quad Ra = \frac{g\beta \Delta T^{(f)}h^3}{\kappa\nu}. \tag{2.10}$$

Note that $\Delta T^{(f)}$ is the temperature difference across the fluid layer, as defined in (2.1), the hydrostatic solution.

A steady, two-dimensional solution of (2.4)–(2.7) and (2.8)–(2.9) can be obtained through the Galerkin expansions

$$\mathcal{X} = \sum_{kln} A_{kln}\mathcal{X}_n(z, \alpha_{kl})\exp(i\alpha(kx + ly)). \tag{2.11}$$

Here $\mathcal{X}$ denotes θ, $\theta^{(u)}$, $\theta^{(l)}$ or ψ. Each expansion term corresponds to a wavelength which is expressed

$$\alpha_{kl} = \alpha\sqrt{k^2 + l^2}. \tag{2.12}$$

The z-dependent trial function $\mathcal{X}_n$ denotes θ_n, $\theta_n^{(u,l)}$ or ψ_n, which must satisfy the boundary equations (2.8) and (2.9). $A_{kln} = A_{-k-ln}^*$ to ensure real-valued solutions, with * denoting the complex conjugate. The summation runs over all integers $-\infty < k, l < \infty$ and $1 \leqslant n < \infty$.

The linear equations (2.6) and (2.7) for $\theta_n^{(l,u)}$ can be solved analytically for each mode (k, l):

$$\theta_n^{(u)}(z, \alpha_{kl}) = -\theta_n\left(\tfrac{1}{2}, \alpha_{kl}\right)\frac{\sinh\left(\alpha_{kl}(z - \tfrac{1}{2} - H)\right)}{\sinh(\alpha_{kl}H)}, \tag{2.13}$$

$$\theta_n^{(l)}(z, \alpha_{kl}) = \theta_n\left(-\tfrac{1}{2}, \alpha_{kl}\right)\frac{\sinh\left(\alpha_{kl}(z + \tfrac{1}{2} + H)\right)}{\sinh(\alpha_{kl}H)}. \tag{2.14}$$

The expansion functions

$$\theta_n(z, \alpha_{kl}) = \frac{\alpha_{kl}K\sin\left(n\pi(z + \tfrac{1}{2})\right) + n\pi\tanh(\alpha_{kl}H)\cos\left((n-1)\pi(z + \tfrac{1}{2})\right)}{\alpha_{kl}K + n\pi\tanh(\alpha_{kl}H)} \tag{2.15}$$

satisfy the boundary conditions (2.9). Using the expansions (2.11), an exact steady solution for each expansion term $\psi_n(z, \alpha_{kl})$ can be found as the solution of the

equation:

$$\left(\frac{\mathrm{d}^2}{\mathrm{d}z^2} - \alpha_{kl}^2\right)^2 \psi_n = Ra\,\theta_n. \tag{2.16}$$

Steady solutions are obtained by solving (2.5) by the use of a Galerkin method resulting in a bilinear system of equations for the unknown coefficients A_{kln}, which can be solved numerically using a Newton–Raphson method. The procedure is similar to that described in Busse (1967).

To determine the stability of the stationary solution infinitesimal disturbances are imposed.

$$\tilde{\mathcal{X}} = \sum_{kln} \tilde{A}_{kln}\mathcal{X}_n(z, \tilde{\alpha}_{kl})\exp(\mathrm{i}(m\alpha + b)x + \mathrm{i}(l\alpha + d)y + \sigma t). \tag{2.17}$$

Here $\tilde{\mathcal{X}}$ is a linear perturbation corresponding to $\mathcal{X}$, where $\mathcal{X}$ denotes θ, $\theta^{(u)}$, $\theta^{(l)}$ or ψ, as before. Furthermore, $\tilde{\alpha}_{kl} = \sqrt{(k\alpha + b)^2 + (l\alpha + d)^2}$ is the wavelength of the disturbance mode. Following Busse (1967), a Galerkin procedure similar to that for the stationary equations is adopted, resulting in an eigenvalue problem, where the growth rate σ assumes the role of an eigenvalue. The largest real part of the growth σ can be determined as a function of b and d. For the case of perfectly conducting slabs, the zigzag and the cross-roll instabilities only involve real-valued σ. In our approach, a linear eigenvalue problem can be obtained only when $\kappa/\kappa^{(s)} = 0$. Note however, that the stability regions obtained using this simplification are valid also for any finite values of $\kappa/\kappa^{(s)}$ provided that the exponential growth, σ, is real-valued corresponding to non-oscillatory instabilities. Additional oscillatory instabilities might exist for some finite value of $\kappa/\kappa^{(s)}$.

3. Steady solutions and their heat transfer

The square cell may be approximately regarded as the intersection of rolls with orthogonal axes. It follows from the symmetries of the solution that no fluid passes through the vertical cell boundaries and the vertical diagonal planes of the cell. The flow and temperatures of a square cell are illustrated by figure 1, for which $K = 0.4$ and $H = 2$. The flow is spreading out from the up-flow in the cell centre and is downwardly directed at the vertical cell side boundaries. The temperature distribution indicates rather strong horizontal temperature gradients in the fluid. The stagnation point locally above the rising fluid is warmer than the stagnation point below the sinking fluid, whereas the temperatures above the sinking fluid and below the rising fluid are approximately equal to the boundary temperatures of the hydrostatic solution.

In order to investigate the dependency of the heat transfer on the thickness and conductivity of the slabs, some selected results showing the Nusselt number as a function of the Rayleigh number will be presented. The heat transport of stationary solutions is described by the Nusselt number

$$Nu = 1 - \left(\frac{\partial\bar{\theta}}{\partial z}\right)_{z=\pm 1/2}, \tag{3.1}$$

where the overbar denotes the horizontal average. The unperturbed motionless solution yields $Nu = 1$, which corresponds to the heat transfer of the hydrostatic solution. The second part of the Nusselt number may be referred to as the convective heat transport. Note that the definition of the Nusselt number, (3.1), is based on a different temperature scale from the one applied by Westerburg & Busse
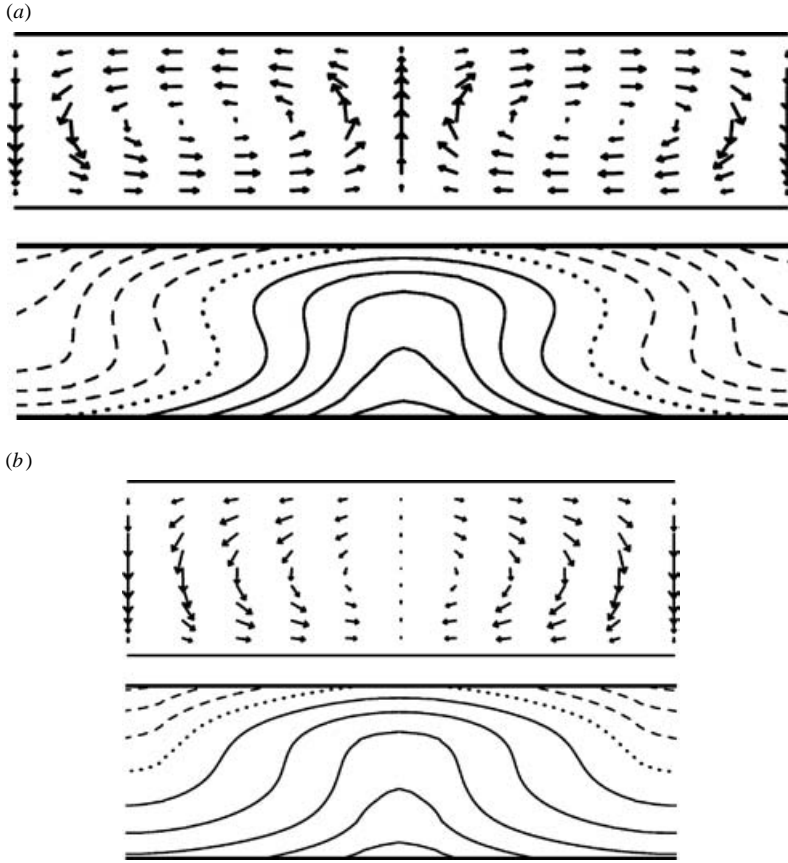
(a)

(b)

FIGURE 1. Velocities and isotherms for squares for $(K, H) = (0.4, 2)$. The wavenumber is the critical, $\alpha_c = 1.6$, and $Ra = 5000$. The two-dimensional vertical sections shown here are planes through which no fluid passes. Seen from above these are: (a) the diagonal square cell section; (b) the square cell sidewall. The difference in value between neighbouring dimensionless isotherms is 0.1.

(2001), who used the difference between the horizontal mean of the temperature at the fluid boundaries. For the special case of symmetric slabs, this scale may be expressed $(1 - 2\bar{\theta}(1/2))\Delta T^{(f)}$. It can be shown that their Nusselt number is equal to $Nu/(1 - 2\bar{\theta}(1/2))$ for cases of symmetric slabs. Even though their scale is of the right order of magnitude, it is inconvenient to apply since it depends implicitly on the realized flow, whereas $\Delta T^{(f)}$ simply involves the prescribed temperatures outside the slabs and the conductivities and the thicknesses of the slabs and the fluid layer. It can be shown that

$$\lim_{K \to 0} Nu = 1 \quad \text{for finite } H, \tag{3.2}$$

$$\lim_{H \to \infty} Nu = 1 \quad \text{for finite } K. \tag{3.3}$$

This reflects that if the fluid layer is very thin compared to the slabs, or the slabs are poorly conducting compared to the fluid, the convection in the fluid layer will not contribute to the overall heat transfer.

Figure 2 shows $Nu - 1$ as a function of $Ra - Ra_c$ for symmetric slabs with $H = 0.1$. The two-dimensional rolls and the three-dimensional squares exhibit approximately
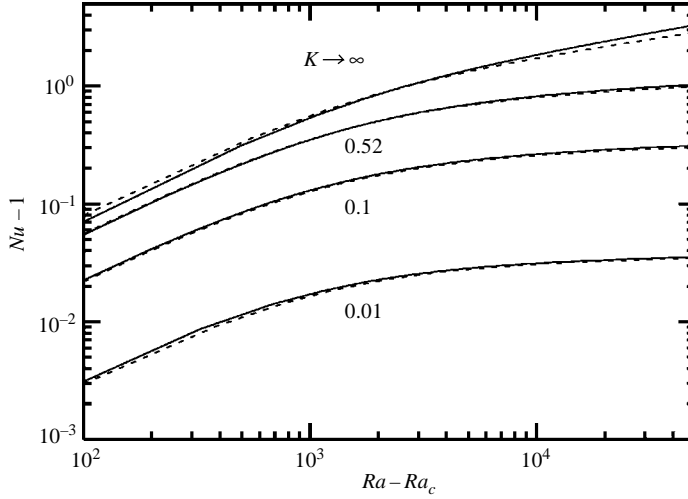
FIGURE 2. The Nusselt number as a function of $Ra - Ra_c$ for cases where the slabs are one-tenth as thick as the fluid layer ($H = 0.1$), and with conductivities as indicated in the figure. The solid (dashed) lines denote squares (rolls).
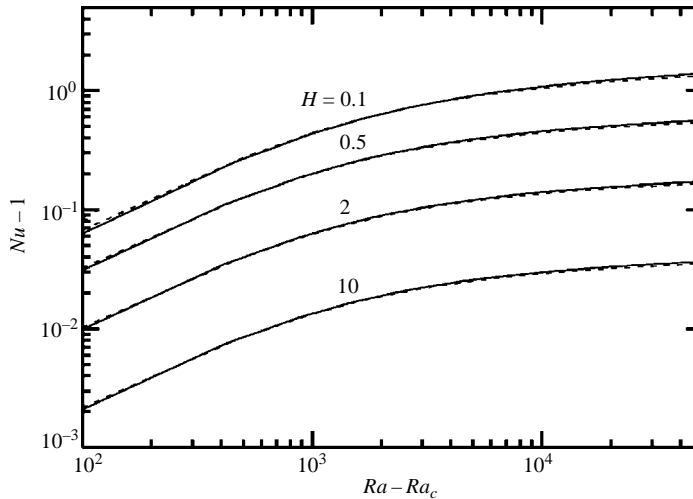

FIGURE 3. The Nusselt number as a function of $Ra - Ra_c$ for cases where the slabs have the same conductivity as the fluid ($K = 1$). The selected values for the thickness of the slabs are as indicated in the figure. The solid (dashed) lines denote squares (rolls).

the same heat transport. The differences are small, but notable. In agreement with the findings of Frick *et al.* (1983) who considered two perfectly conducting slabs, it is found here that the asymptotic power law for the Nusselt–Rayleigh number relationship appears to be distinctly different for squares than for rolls at Rayleigh numbers larger than about 5000. The Nusselt number is larger for squares than for rolls for all the slab selections at sufficiently large Rayleigh numbers. This distinction almost disappears for the slab selections with lower conductivities. For small Ra the stable solution yields the largest Nu (in agreement with the weakly nonlinear theory, Holmedal *et al.* 2005). In figure 3, the conductivity of the slabs is chosen equal to the

conductivity of the fluid. The Nusselt number decreases significantly with increased thickness of the slabs.

It follows from the discussion above that the heat transfer in the case of infinitely thick slabs by Westerburg & Busse (2001) is not at all influenced by the convection in the fluid layer. From (3.3), it is realized that the change of their Nusselt number is related entirely to the change of their temperature scale, namely the difference between the mean temperatures at the fluid boundaries, which depends not only on the prescribed outer temperature difference, ΔT, but also on the steady solution itself. Our findings reveal that the dependency on the slab thickness and thermal conductivity is indeed strong.

4. Stability regions

A selection of Busse balloons for the case of two symmetric slabs of thickness $H = 0.1$ is shown in figure 4. The disturbance wavenumber of the cross-roll instability is close to the critical wavenumber except at the largest Rayleigh numbers. The balloons are shifted towards smaller wavenumbers with decreased conductivity of the slabs. As was found for cases of infinitely thick slabs by Westerburg & Busse (2001), the balloons shrink towards the critical point and vanish for sufficiently small K. The rolls are replaced by squares at $K = 0.2356$ (calculated using the weakly nonlinear theory). The results with $H = 0.1$ suggest that cases of thin poorly conducting slabs might remain stable at even larger Rayleigh numbers. In such cases, only one slab parameter is necessary, namely K/H. This limit will be omitted here, because the numerical implementation has not been designed to cope with this limit with a sufficient accuracy.

Westerburg & Busse (2001) showed, for cases of infinitely thick slabs, that the largest stability region was obtained with perfectly conducting slabs. Accounting for their use of a definition of the Rayleigh number based on the difference between the mean temperatures at the fluid–slab interfaces does not change this. Their Rayleigh number may be expressed $(1 - 2\bar{\theta}(1/2))Ra$. It becomes equal to the one adopted here for the case of perfectly conducting boundaries.

As was pointed out by Frick *et al.* (1983), it is sufficient to consider disturbances with wavenumbers b and d in a triangular region enclosed by the lines $b = d$, $d = 0$ and $d = \alpha/2$ when studying the stability of the square solutions. It turns out that the most unstable perturbations are always found for small values of b and d.

Figure 5 shows the stability region for convection in the form of squares for a slab selection corresponding to the experiment by Le Gal *et al.* (1988). Certainly, squares are the preferred pattern for this case according to weakly nonlinear theory (Holmedal *et al.* 2005). However, their measured wavenumber, $\alpha = 2.5$ at Rayleigh numbers around 2000, is located on the right-hand side outside the stability region in the figure. The disagreement is most probably due to a finite Prandtl number ($Pr = 7$) in their experiment.

Three types of instability delineate the stability boundaries of stable squares in figure 5. The long wavelength cross-roll instability (LW-CR) and the square-zigzag instability (SZZ) have been calculated by the stability analysis with the Ginzburg–Landau equations as described in Holmedal *et al.* (2005) and are included with the dashed lines in the figure. Note that the SZZ boundary vanishes to the left immediately above the critical point. However, the behaviour very close to the critical point for the onset of convection agrees with the predictions of the weakly nonlinear theory, as can be seen from the enlargement of the region close to the critical point inserted
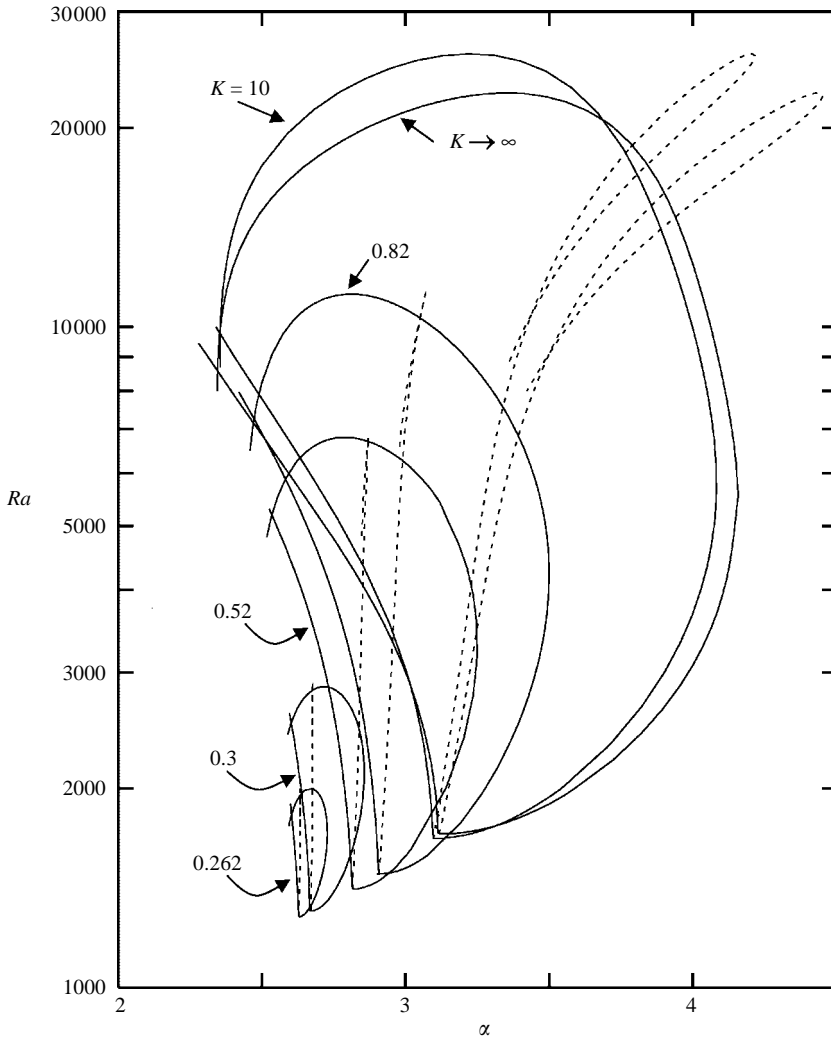
FIGURE 4. Two-dimensional rolls are stable in the closed regions. The thickness of the slabs is $H = 0.1$ and K is as indicated on the figure. The wavenumber (d) of the most rapidly growing disturbance (cross-roll) is indicated by the dashed curves in the figure.

in figure 5. The LW-CR boundary is predicted correctly by the weakly nonlinear theory in the range $(Ra - Ra_c)/Ra_c < 0.2$. In addition, a new type of instability is revealed at the upper left-hand boundary of the balloon. This instability is labelled the roll-competition instability (RC) because it energizes the planform modes of the squares, $\tilde{A}_{101}$, $\tilde{A}_{-101}$, $\tilde{A}_{011}$ and $\tilde{A}_{0-11}$.

In figure 6, the largest growth rates of the eigensolutions are shown for perturbations with $d = b$. The point $(Ra, \alpha) = (5600, 1.82)$ is considered for slabs with $H = 2$ and $K = 0.4$. This choice of the parameters corresponds to a point placed right above the RC boundary in figure 5. Considering very small values of d/α, the three largest eigenvalues are close to each other but distinct. The largest growth is obtained for $d \rightarrow 0$. The second largest eigenvalue (LW-CR) and the largest eigenvalue (RC) are merged into a complex conjugate pair of eigenvalues as d/α is increased above a
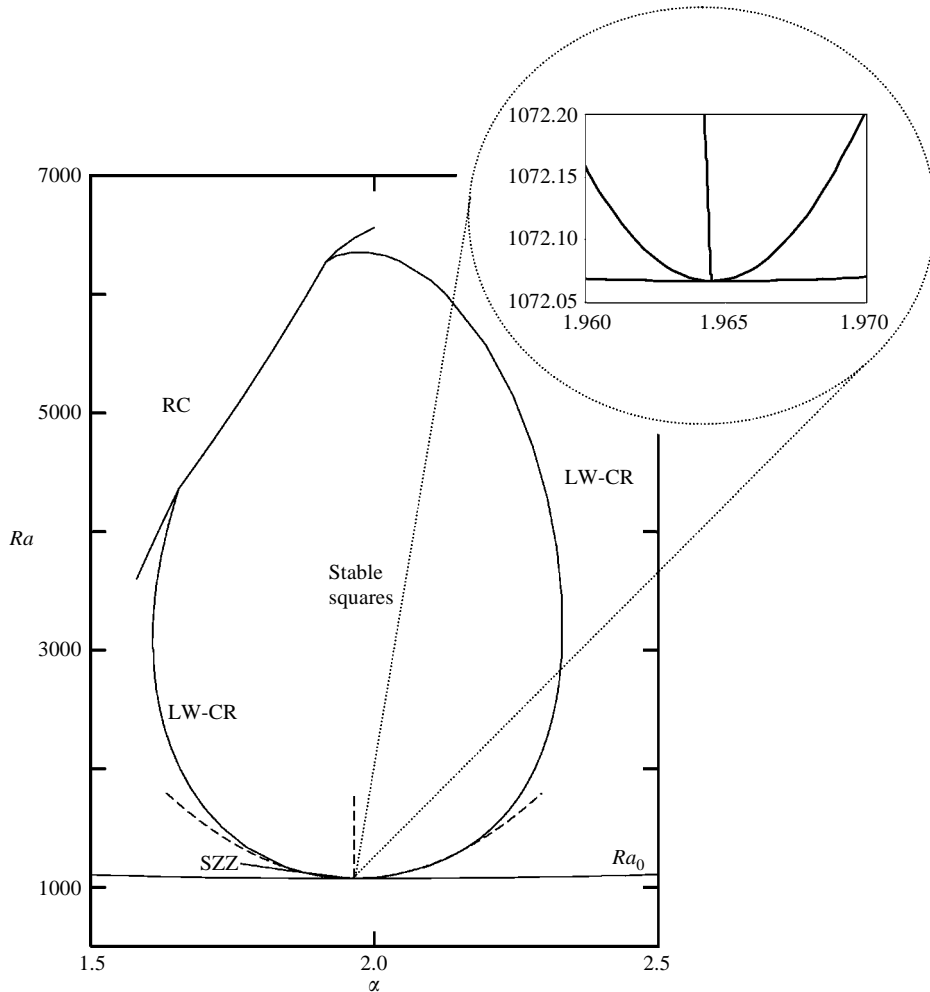
FIGURE 5. Three-dimensional squares are stable in the closed region. The two slabs are symmetric with $H = 2$ and $K = 0.4$ (Plexiglas and water). The long wavelength cross-roll instability (LW-CR), the square-zigzag instability (SZZ) and a new instability, which we denote the 'roll-competition' instability (RC), yield the stability boundaries. The dashed lines show the boundaries predicted by weakly nonlinear theory. An enlargement of the region close to the critical point is included.

certain value. The real part of this pair of eigenvalues remains positive in a range of small d/α. Thus, instabilities with both real and complex growth rates may arise within a finite bandwidth.

The closer the approach to the RC boundary, the smaller is the region where the two largest eigenvalues are distinct. Exactly at the RC boundary, the LW-CR instability and the RC instability exchange places. Below the RC boundary, the region of distinct real eigenvalues increases again, the LW-CR instability being the largest (stable).

Westerburg & Busse (2001) reported the coexistence of rolls and squares in an experiment with silicon oil of a high Prandtl number and with transparent slabs. Their set-up corresponds to $K = 1.18$ and $H = 2.5$. In figure 7, such regions are shown
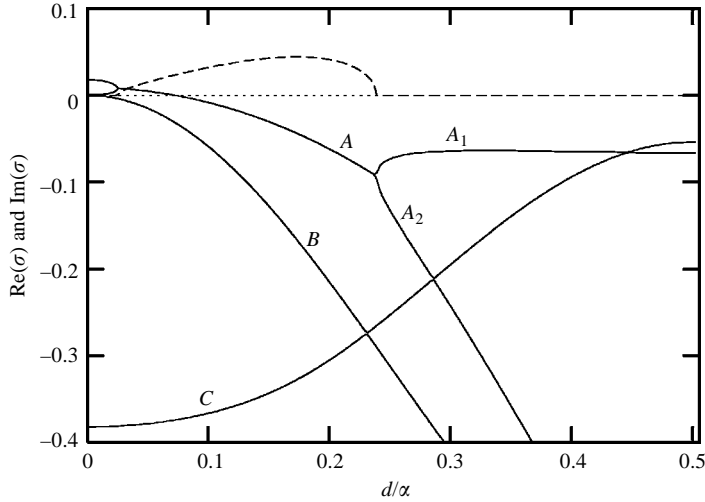
FIGURE 6. The dependency of the largest eigenvalues on d/α along the line $d = b$. A point of unstable squares right outside the RC instability boundary is considered, for the slab parameters $H = 2$ and $K = 0.4$ (Plexiglas and water), and $(Ra, \alpha) = (5600, 1.82)$ as indicated by an arrow in figure 5. The dashed line denotes the absolute value of the imaginary part of the complex conjugate pair of eigenvalues with the real part labelled A. This pair of eigenvalues splits into two real-valued eigenvalues A_1 and A_2. The eigenvalue labelled C is the largest one for $d/\alpha > 0.44$.

for the case of infinitely thick slabs with $K = 1.1$. Rolls are stable in a region above the critical point, $Ra_c < Ra < Ra_2$, where Ra_2 is the uppermost Rayleigh number for stable rolls. In the figure, the lowermost Rayleigh number for stable squares is smaller than Ra_2. Thus, for a small range of Rayleigh numbers below Ra_2, rolls and squares may both be stable at the same set-up, but for slightly different wavenumbers, because these two stability regions in the figure are distinct. Note that this overlap of the wavenumbers is in the same range of Rayleigh numbers as reported by Westerburg & Busse (2001). Note also that the relatively narrow bandwidths of stable wavenumbers for rolls and for squares are very close to each other and to α_c. Hence, a hysteretic transition is not necessary to explain their coexistence.

Figure 8 shows four regions for stable squares, for which the thickness of the slabs is $H = 0.1$. The conductivities are all smaller than $K = 0.2356$, which is the largest value where the critical point for onset of convection is a part of the stability region for squares. Hence, the weakly nonlinear theory is valid, as indicated by the dashed curves in the figure. The stability region in the figure which contains the largest Rayleigh number for stable squares is obtained for $K = 0.1$. The heights of the stability regions decrease and the widths increase for the selections with lower values of K than this. The LW-CR instability displaces the RC instability progressively as the conductivity of the slabs is reduced. However, the RC instability is still present for the case considered with $K = 0.001$.

Figure 9 indicates two more examples of stability regions of rolls and squares for the same slab thickness $H = 0.1$ as in figure 8. Since here the conductivities ($K = 0.262$ and 0.269) are larger than $K = 0.2356$, the onset of convection is in the form of rolls. The tiny region of stable squares obtained with $K = 0.269$ represents about the largest value of K, for which this pattern is stable when $H = 0.1$. Note that the Busse balloon
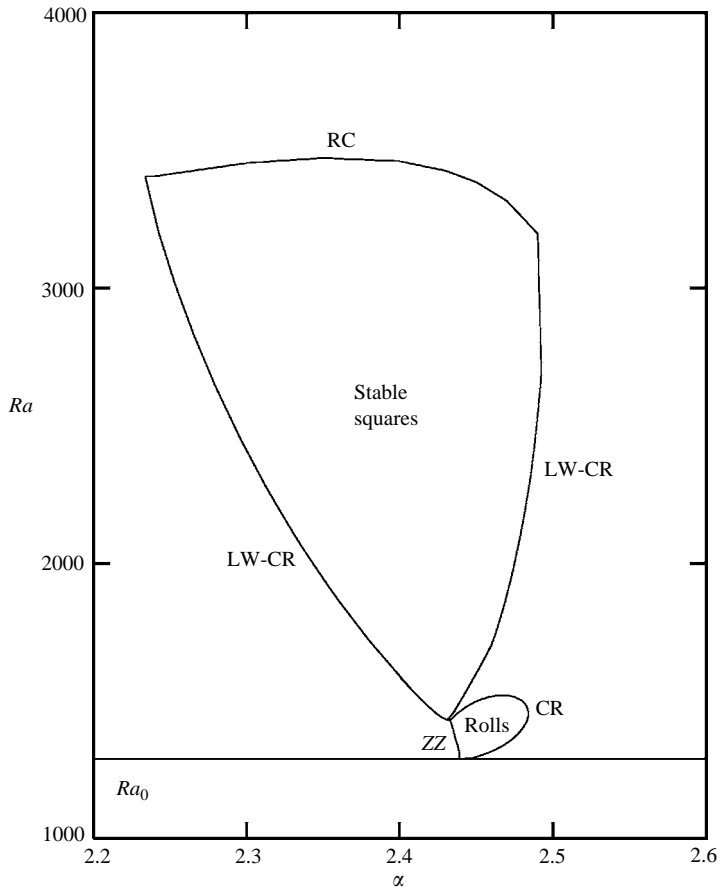
FIGURE 7. The stability regions of three different solutions for the case with infinite thickness and $K = 1.1$. The motionless basic state is stable below the neutral stability curve, Ra_0. At supercritical Rayleigh numbers the rolls are stable in the Busse balloon located right above the critical point. Squares are stable in the uppermost closed region.

and the stability region of squares in these two cases are separated by an interval of the Rayleigh number, within which none of these patterns are stable.

5. Summary and conclusions

Steady squares and rolls in Rayleigh–Bénard convection between symmetric slabs, their heat transfer and their stability have been calculated numerically. The heat transfer depends strongly on the thickness and the conductivity of the slabs. That the stable pattern yields the strongest heat transfer is true only in the weakly nonlinear range.

Examples of stability regions of both rolls and squares have been calculated. In one case, with a slab that is one tenth as thick as the fluid layer and with a ten times better thermal conductivity, the largest Rayleigh number where the rolls are still stable is larger than for the case of perfectly conducting boundaries. As the thermal conductivity of the slabs is reduced, the stability region of the rolls shrinks onto the critical point for onset of convection.
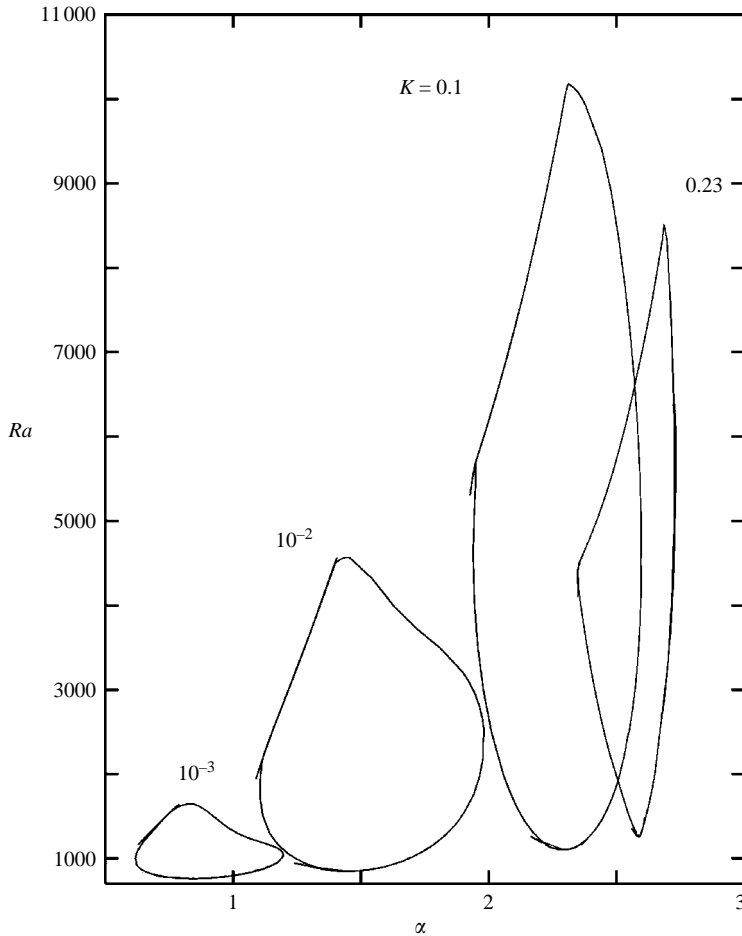
FIGURE 8. Squares are stable in the closed regions. For all the four cases the slabs aresymmetric with $H = 0.1$. The conductivities of the slabs, K, are indicated in the figure.

In agreement with weakly nonlinear theory (Holmedal *et al.* 2005) the long wavelength cross-roll instability and the square zigzag instability are responsible for the stability borders in the lower part of the stability region of three-dimensional squares. A new type of instability occurs at larger Rayleigh numbers. At a thermal conductivity of the slabs slightly above the limit where stable rolls appear, the stability region of squares shrinks onto a point at a supercritical Rayleigh number.

Examples are calculated where the rolls are stable close to onset and squares are stable in a closed region at slightly larger Rayleigh numbers. However, no overlap between such regions has been found in the calculated examples. This provides an explanation for the observed coexistence of squares and rolls by Westerburg & Busse (2001).

Finally, some future perspectives: dependent on the slab properties, combinations of stable rolls, squares and hexagons are possible solutions in the early nonlinear regime. Additional viscous instabilities will occur at finite Prandtl numbers. The large stability regions obtained with the thin slabs are an interesting topic. The set-up investigated here is simple and relevant for experimental conditions. It gives rise to
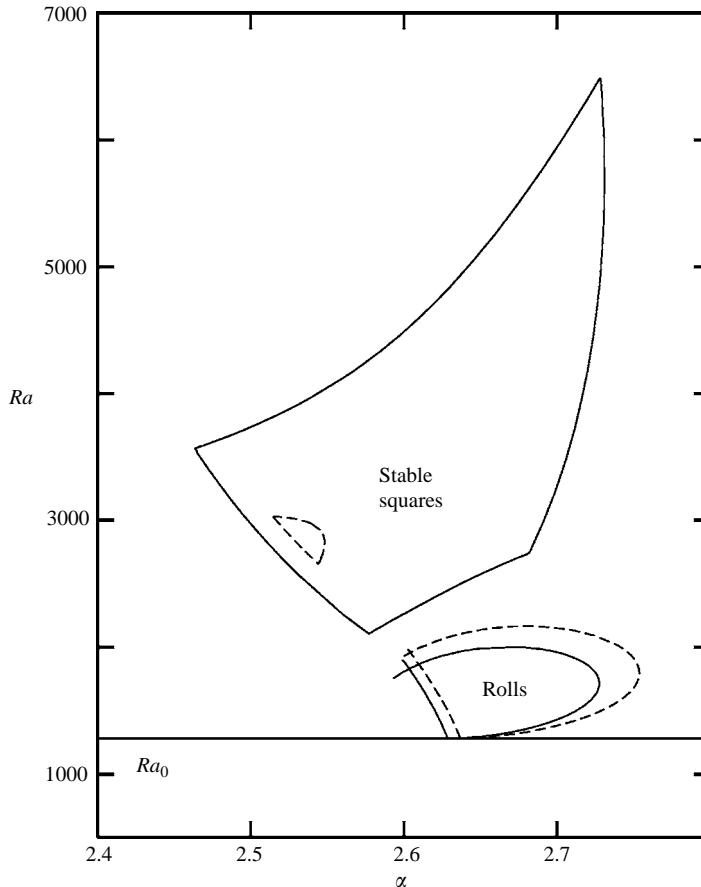
FIGURE 9. The stability regions of the steady solutions for slabs with $H = 0.1$. Solid lines denote $K = 0.262$ and dashed lines denote $K = 0.269$. The motionless basic state is stable below the neutral stability curve Ra_0. Rolls are stable in the Busse balloon, which is located right above the critical point. Squares are stable in the uppermost closed region.

a rich varity of instabilities and may still serve as an ideal case for many future investigations of instability mechanisms and pattern formation.

REFERENCES

BUSSE, F. H. 1967 On the stability of two-dimensional convection in a layer heated from below. *J. Math. Phys.* **46**, 140–149.

BUSSE, F. H. & RIAHI, N. 1980 Nonlinear convection in a layer with nearly insulating boundaries. *J. Fluid Mech.* **96**, 243–256.

CLEVER, R. M. & BUSSE, F. H. 1996 Hexagonal convection cells under conditions of vertical symmetry. *Phys. Rev.* E **53**, 2037–2040.

FRICK, H., BUSSE, F. H. & CLEVER, R. M. 1983 Steady three-dimensional convection at high Prandtl numbers. *J. Fluid Mech.* **127**, 141–153.

GETLING, A. V. 1998 Rayleigh–Bénard Convection: Structures and Dynamics. *World Scientific.*

HOLMEDAL, B., TVEITEREID, M. & PALM, E. 2005 Planform selection in Rayleigh–Bénard convection between finite slabs. *J. Fluid Mech.* **537**, 255–270.

HOYLE, R. B. 1993 Long wavelength instabilities of square patterns. *Physica* D **67**, 198–223.

LE GAL, P., POCHEAU, A. & CROQUETTE, V. 1988 Appearance of a square pattern in a Rayleigh–Bénard experiment. *Phys. Fluids* **31**, 3440–3442.

PROCTOR, M. R. E. 1981 Planform selection by finite-amplitude thermal convection between poorly conducting slabs. *J. Fluid Mech.* **113**, 469–485.

WESTERBURG, M. & BUSSE, F. 2001 Finite-amplitude convection in the presence of finitely conducting boundaries. *J. Fluid Mech.* **23**, 129–144.